A Detailed Evaluation of Model Defects as Candidates for the Bias Temperature Instability

F. Schanovsky, O. Baumgartner, W. Goes, and T. Grasser
Institute for Microelectronics, TU Wien
Gußhausstraße 27-29/E360, 1040 Wien
Fax: +43/1/58801-35099

***Abstract*—Despite its long research history, the bias temperature instability (BTI) is still not fully understood. Recent advances on both the experimental and theoretical side have deepened our understanding of the phenomenon, but the microscopic origin is still unknown. We report on a detailed evaluation of atomistic models of the oxygen vacancy and the hydrogen bridge defects in SiO_2 as candidates for the defect responsible for the BTI. For this purpose, time constants are calculated using a combination of atomistic and semiconductor device modeling. These time constants are then compared to electrical measurement data obtained from BTI experiments on individual defects in small-area MOS transistors. The inherent uncertainty in the energetic position of the energy levels in the density functional calculation with respect to the device simulation is accounted for using an empirical energy shift. Very good agreement with the experimental data is found for the hydrogen bridge defect, while for the oxygen vacancy severe discrepancies between the predicted behavior and the experimental observation arise.**

I. Introduction

The bias temperature instability (BTI) of metal-oxide-semiconductor (MOS) transistors is currently one of the hottest topics of semiconductor reliability research. Although the BTI research history dates back to the mid-sixties, the understanding of this effect is still incomplete. The currently most successful model for BTI is the multi-state multi-phonon model [1], [2]. In this theory, the recoverable component of the BTI arises from the charging of point-defects in the oxide of the MOS structure. During BT stress, these defects assume a positive charge state and also undergo a structural reorganization that changes their bonding structure as well as their trapping behavior.

The time-dependent defect spectroscopy (TDDS) [1], [2], is an experimental technique which is based on the detailed analysis of steps in the recovery traces of nanoscale transistors after BTI stress. This method makes the study of the capture and emission behavior of single defects possible. The charging and discharging time constants obtained from these experiments can be well explained using the multi-state NMP model, even for complex scenarios like AC stress [3].

The success of the multi-state NMP model has led to interest in the atomic structure at its heart, i.e. the defect causing the BTI. Unfortunately, as of today the experimental evidence in this direction is weak. We try to shed some light on the atomistic structure of the BTI defect based on theoretical calculations. For this purpose we calculate the TDDS response of two defect candidates using a combination of macroscopic device simulation and atomistic defect models.

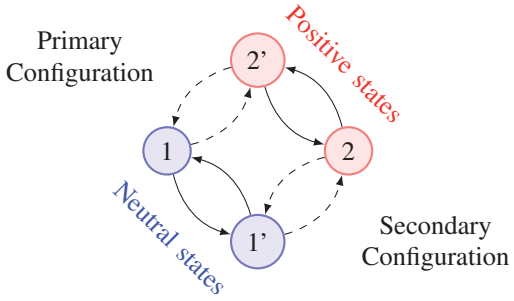

Fig. 1. The BTI defect has (at least) two stable structural configurations, which can assume a neutral and a positive charge state. The structural reconfigurations are barrier-hopping transitions (⟶) and the transitions between different charge states are non-radiative multi-phonon transitions (⇢).

II. Defect States

The defect at the heart of the multi-state multi-phonon model for BTI has a total of four (dominant) states. Those states arise from two charge states 1 (neutral) and 2 (positive), in which the defect assumes one of two structural configurations, see Fig. 1. The states themselves as well as the transition rates between the states are determined by the potential energy surfaces of the BTI defect [4]. For each charge state, the more stable structural configuration, i.e. the configuration with lower total energy, is referred to the unprimed state (1,2), and the less stable configuration is referred to the primed state (1′,2′).

While the potential energy surfaces of the BTI defect are usually calibrated to experimental data, in the present work we extract the relevant parameters from density functional calculations. The atomistic defect models employed for this purpose are based on a crystalline SiO_2 supercell structure [5], [6]. The defect candidates investigated in our work are the oxygen vacancy and the hydrogen bridge [5], [7]. Both defects have been studied in the context of MOS reliability [6], [8] and are known to have two stable configurations in the neutral and the positive state. The assignments of the structural configurations to the BTI defect states are based on the relative energies of the defects as obtained from DFT. In accord with the model assumptions, for every charge state the less stable configuration is the primed state and the other is the unprimed state, see Fig. 2. More details on the DFT part can be found elsewhere [5].

III. Elementary Reactions

As shown in Fig. 1, the BTI defect undergoes two types of transitions: the structural reconfigurations ($1 \leftrightharpoons 1'$, $2 \leftrightharpoons$

978-1-4673-5736-4/13/$31.00 ©2013 IEEE

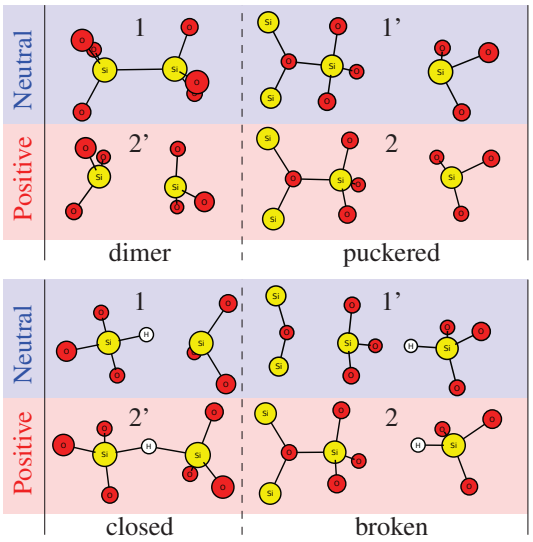

Fig. 2. The considered states of the oxygen vacancy (top) and the hydrogen bridge (bottom). The identification of the structural configurations of the atomistic models with the states of the BTI defect is based on their relative energy.

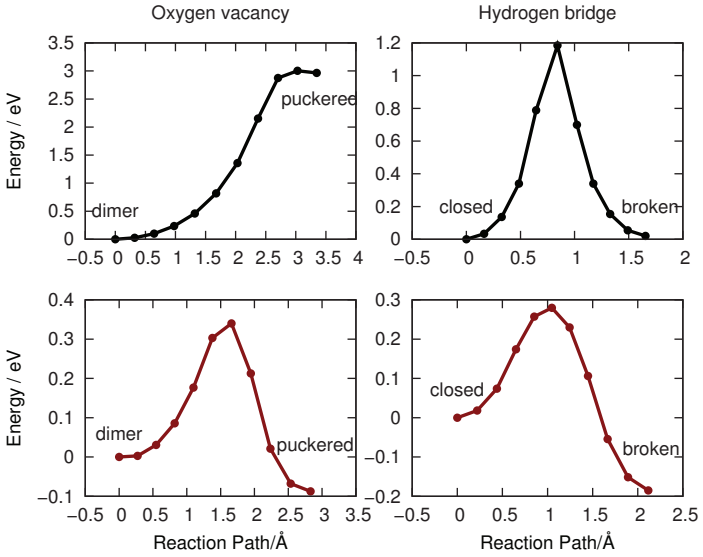

Fig. 3. The reaction paths for the $1 \rightleftharpoons 1'$ (top) and $2 \rightleftharpoons 2'$ (bottom) transitions as obtained using the nudged-elastic band method.

$2'$) and the charge state transitions ($1 \leftrightharpoons 2'$, $1' \leftrightharpoons 2$). In the present work, the structural reconfigurations, which are understood as barrier hopping transitions, are modeled using the simple expression

$$\tau_{\alpha\beta} = \nu \exp(-\frac{E_{\alpha\beta}}{k_{\mathrm{B}}T}), \tag{1}$$

where $(\alpha, \beta) \in \{(1,1'),(1',1),(2,2'),(2',2)\}$ and the attempt frequency ν is an adjustable parameter. The activation energy $E_{\alpha\alpha'}$ is calculated from the atomistic model using the nudged elastic band method as implemented in the VASP package [9]. The energies along the calculated reaction paths are shown in Fig. 3. The hydrogen bridge shows reasonable agreement with the BTI defect values [10] both in the neutral and the positive state. For the oxygen vacancy, the $2 \rightleftharpoons 2'$ barriers are also close to the experimental estimates, but a strong discrepancy arises for the $1 \rightleftharpoons 1'$ barriers. The barrier of about $36\mathrm{meV}$ for the transition from the puckered to the dimer configuration is much too small for BTI. However, this may be an artifact of the crystalline host structure, as higher barriers have been reported [11] for the oxygen vacancy in amorphous silica.

The charge state transitions of the BTI defect are non-radiative multi-phonon (NMP) transitions. These are described using

$$k_{n\to\mathrm{d}} = \lambda \int_{-\infty}^{\infty} n(\vec{r}_{\mathrm{d}}, E) f_{\beta}^{(+/0)}(E) dE, \tag{2}$$

$$k_{p\to\mathrm{d}} = \lambda \int_{-\infty}^{\infty} p(\vec{r}_{\mathrm{d}}, E) f_{\alpha}^{(0/+)}(E) dE, \tag{3}$$

$$k_{\mathrm{d}\to n} = \lambda \int_{-\infty}^{\infty} (D_n(\vec{r}_{\mathrm{d}}, E) - n(\vec{r}_{\mathrm{d}}, E)) f_{\alpha}^{(0/+)}(E) dE, \tag{4}$$

$$k_{\mathrm{d}\to p} = \lambda \int_{-\infty}^{\infty} (D_p(\vec{r}_{\mathrm{d}}, E) - p(\vec{r}_{\mathrm{d}}, E)) f_{\beta}^{(+/0)}(E) dE, \tag{5}$$

where $k_{n\to\mathrm{d}}$ and $k_{p\to\mathrm{d}}$ are the rates for electron and hole capture, $k_{\mathrm{d}\to n}$ and $k_{\mathrm{d}\to p}$ are the rates for electron and hole emission. The densities n, p, D_n and D_p are the occupied

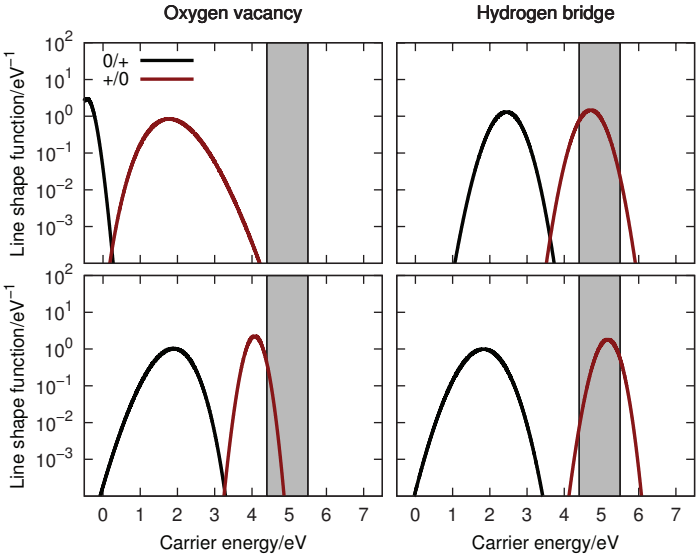

Fig. 4. The charging and discharging line shapes for the reactions $1 \rightleftharpoons 2'$ (top) and $2 \rightleftharpoons 1'$ (bottom). Energies are relative to the SiO_2 valence band edge, the band-gap of the silicon bulk is indicated as grey area.

and total densities for the electrons and holes in the MOS structure. λ is a free parameter, and $f_{\alpha}^{(0/+)}$ and $f_{\beta}^{(+/0)}$ are the line shapes for charging and discharging the defect ($\alpha \in \{1,1'\}$, $\beta \in \{2,2'\}$), respectively. The line shapes are calculated from the density functional defect models using a recently developed extraction method [5]. The charging and discharging line shapes calculated for our candidate defects are shown in Fig. 4. One can see a striking difference in the charging behavior of the dimer and the puckered state of the oxygen vacancy, while this difference is much less pronounced for the closed and broken hydrogen bridge. The position of the $f^{(0/+)}$ maximum of the oxygen vacancy dimer is close to the SiO_2 valence level, in agreement with the switching trap level for that transition [6]. A $f^{(0/+)}$ line shape at this energetic position makes a hole capture from the Si valence level very unlikely, even under large bias. The charging line shapes of

the hydrogen bridge are much closer to the Si valence level making a charging transition under bias more likely.

The carrier densities are taken from a non-equilibrium Green's function device calculation of the MOS structure [7], [12], The device structure consists of a poly-Si gate and an n-doped bulk separated by a $2.2\,\mathrm{nm}$ SiO_2 layer. For the device calculation as well as for the capture and emission rates, we consider the unprimed and primed electron valleys, as well as the heavy-hole and light-hole bands. The contributions from the different valleys are combined to obtain the total charging time constants ($\tau_{12'}$, $\tau_{1'2}$) and discharging time constants ($\tau_{21'}$,$\tau_{2'1}$).

IV. Capture and Emission Time Constants

The effective charging (capture) time constant τ_c and discharging (emission) time constant τ_e, which are measured using the TDDS technique [1], [2] are calculated from the time constants of the elementary reactions as [13]

$$\tau_\mathrm{c} = \tau_{12'} + \tau_{2'2}\left(1 + \frac{\tau_{12'}}{\tau_{2'1}}\right), \tag{6}$$

$$\tau_\mathrm{e} = \frac{1}{\tau_{\mathrm{e}1}^{-1} + \tau_{\mathrm{e}2}^{-1}}, \tag{7}$$

$$\tau_{\mathrm{e}1} = \tau_{22'} + \tau_{2'1}\left(1 + \frac{\tau_{22'}}{\tau_{2'2}}\right), \tag{8}$$

$$\tau_{\mathrm{e}2} = \tau_{21'} + \tau_{1'1}\left(1 + \frac{\tau_{21'}}{\tau_{1'2}}\right). \tag{9}$$

The effective time constants τ_c, $\tau_{\mathrm{e}1}$, and $\tau_{\mathrm{e}2}$ correspond to the reaction paths $1 \to 2' \to 2$, $2 \to 2' \to 1$, and $2 \to 1' \to 1$, respectively.

V. Energy Alignment

The largest uncertainties in our calculations originate from the inherent difficulty to align the total energies calculated from DFT to the single-electron energies present in the device calculation. Different approaches to this problem have been used in the literature [14]. However, all of these methods have inherent uncertainties of unknown magnitude, that might be as large as $\pm 0.5\,\mathrm{eV}$ [6]. Additionally, our results strongly depend on the Si-SiO_2 valence band offset, as the line shapes are referenced to the SiO_2 valence level. The valence band offset in our calculations is $4.4\,\mathrm{eV}$, but values from $4.2\,\mathrm{eV}$ to $4.8\,\mathrm{eV}$ have been given in the literature [15]. In the present work we take these uncertainties as another degree of freedom for our calculations. We establish the basic relation between the total energies obtained from DFT and the single-electron energies in the device calculation by aligning the valence level of the Kohn-Sham auxiliary system to the SiO_2 valence level of the device calculation. Additionally we introduce an energetic correction ΔE, that accounts for the uncertainties in the energy alignment, as another adjustable parameter besides ν_α and λ. This energetic correction shifts the alignment to account for the inherent inaccuracies of the Kohn-Sham system and the Si-SiO_2valence band offset. A positive ΔE shifts the line shapes towards more positive energies in the band diagram. Fig. 5 shows the impact of different alignment corrections on the elementary reactions $1 \leftrightharpoons 2'$ of the hydrogen bridge.

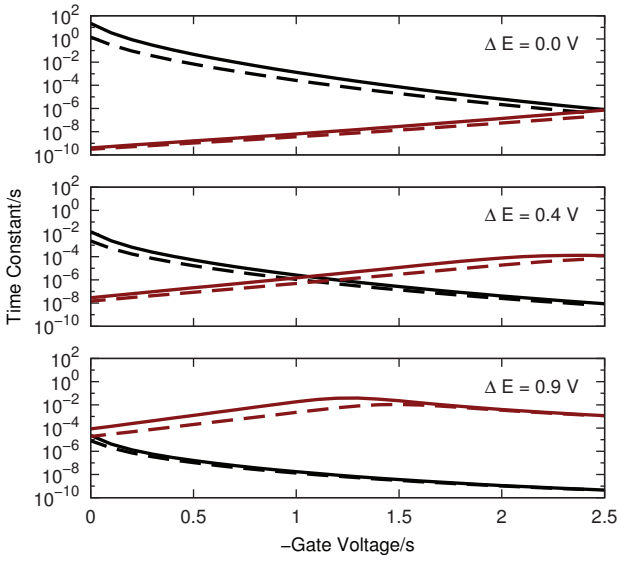

Fig. 5. Influence of the energy alignment on the time constants $\tau_{12'}$ (black) and $\tau_{2'1}$ (red) for $400\,\mathrm{K}$ (solid) and $450\,\mathrm{K}$ (dashed). Relatively small variations of the alignment lead to strong changes in the capture and emission behavior.

We estimate the uncertainties in the energy alignment to about $\pm 0.7\,\mathrm{eV}$, which severely affects the calculated rates. The introduction of the empirical correction parameter ΔE accounts for these uncertainties and moves the focus of the evaluation to the shapes of the DFT-potentials, which are usually more accurate than their alignment.

VI. Results

To evaluate our atomistic model defects as BTI defect candidates we compare the calculated effective time constants τ_c and τ_e to extractions from TDDS. Very detailed TDDS data for a p-channel MOSFET have been published in [4]. The experimentally observed τ_c varies over several orders of magnitude, but always shows a strong dependence on the applied gate voltage. With regard to the discharging rate τ_e, some defects show little to no gate voltage dependence, while others show an increasing emission rate towards more positive gate voltages. In the TDDS experiments every defect shows different temperature and field activation of the capture and emission time constants. These differences arise because the defects in the amorphous MOS oxide reside in different structural environments that lead to different activation energies for both the reconfigurations and the charge transitions. We thus not attempt a direct fit of our theoretical models to the experimental data but draw our conclusions on the reasonability of the atomistic defect candidate from the qualitative reproduction of the experimental behavior.

Fig. 6 compares the calculated time constants to experimental data. For the hydrogen bridge $\Delta E = 0.4\,\mathrm{eV}$, $\nu = 10^8\,\mathrm{s}^{-1}$, $\lambda = 2\pi/h$ gives excellent agreement with the experimental data. Fig. 7 shows the time constants for the elementary reactions of the hydrogen bridge for this parameter set.

The oxygen vacancy requires $\Delta E = 4\,\mathrm{eV}$ to obtain reasonable τ_c, as the charging line shape in the dimer (1) state is quite narrow and has its maximum around the SiO_2 valence

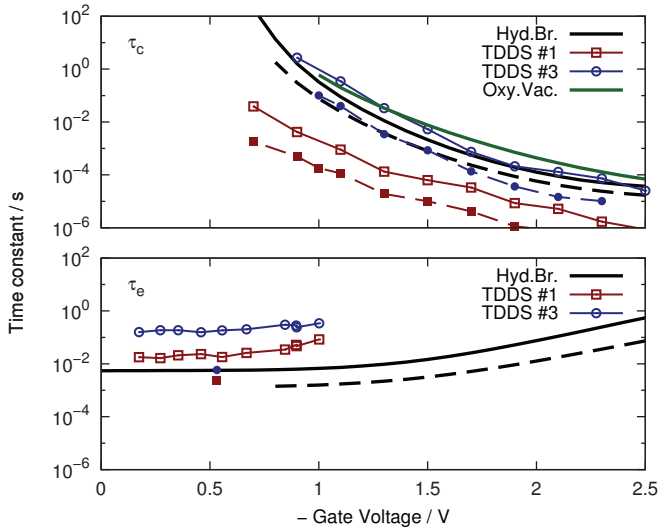

Fig. 6. Comparison of the calculated capture (top) and emission (bottom) time constants to experimental data (the numbers indicate the original defect index [4]) for 400 K (solid lines, open symbols) and 450 K (dashed lines, filled symbols). The hydrogen bridge shows excellent agreement for a moderate energetic correction and reasonable λ and ν. For the oxygen vacancy, in order to obtain a reasonable τ_c, an enormous correction is required, due to the unfavorable position of the charging line shape in the dimer state.

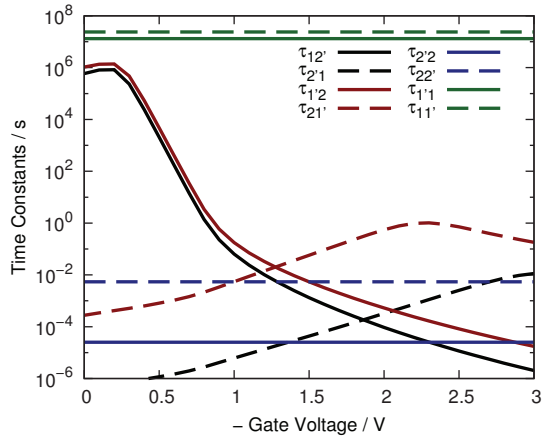

Fig. 7. The time constants for the elementary reactions of the hydrogen bridge at 400 K.

level. At this alignment correction, however, $f^{(+/0)}$ of the puckered (2) state moves deeply into the conduction band and a neutralization of the defect becomes effectively impossible.

VII. Conclusion

We report on a detailed comparison of atomistic model defects to experimental data obtained from electrical measurements. The defects investigated are the hydrogen bridge and the oxygen vacancy. Our calculations have a small number of free parameters which keep the theoretical model as simple as possible. Additionally, an empirical energy correction is introduced to account for errors in the alignment of the total DFT energies and the single-electron energies in the device.

The oxygen vacancy model used in this work requires an unreasonably high energy correction to obtain a reasonable behavior of τ_c. Just like the low barrier for the transition from the puckered to the dimer configuration, this could be an artifact of the crystalline host structure. However, Gös et al. have calculated switching trap levels for oxygen vacancies in amorphous silica [16] and have found a very small spread in the distribution of these levels for the investigated samples. The switching trap level is the zero-temperature limit of the line shape. One can thus assume that the position of the charging line shape of the oxygen vacancy dimer configuration is only weakly influenced by the surrounding atoms. Consequently, this structure cannot be considered a likely candidate for the state 1 of the BTI defect even if a disordered host structure is considered. Very good agreement with the experimental data is found on the other hand for the hydrogen bridge defect using a comparably small energy correction and a reasonable set of parameters. Furthermore, it has been reported that the switching trap levels of the hydrogen bridge in amorphous silica show a wide distribution in energy, indicating a stronger dependence on the structural environment [16]. All in all, this makes the hydrogen bridge a good candidate for the BTI defect.

VIII. Acknowledgement

This work has received funding from the EC's FP7 grant agreement NMP.2010.2.5-1 (MORDRED).

References

[1] T. Grasser *et al.*, "Advanced Characterization of Oxide Traps: The Dynamic Time-Dependent Defect Spectroscopy," in *Proc. Intl.Rel.Phys.Symp.*, apr 2013.

[2] T. Grasser *et al.*, "Time-Dependent Defect Spectroscopy for Characterization of Border Traps in Metal-Oxide-Semiconductor Transistors," *Phys. Rev. B*, vol. 82, pp. 245 318–1, 2010.

[3] T. Grasser *et al.*, "On the frequency dependence of the bias temperature instability," in *Proc. Intl.Rel.Phys.Symp.*, 2012, pp. XT.8.1–XT.8.7.

[4] T. Grasser *et al.*, "The Time Dependent Defect Spectroscopy (TDDS) for the Characterization of the Bias Temperature Instability," in *Proc. Intl.Rel.Phys.Symp.*, 2010, pp. 16–25.

[5] F. Schanovsky *et al.*, "An Advanced Description of Oxide Traps in MOS Transistors and its Relation to DFT," *J.Comp.Elect.*, vol. 9, pp. 135–140, 2010.

[6] P. E. Blöchl, "First-principles calculations of defects in oxygen-deficient silica exposed to hydrogen," *Phys. Rev. B*, vol. 62, no. 10, pp. 6158–6178, September 2000.

[7] F. Schanovsky *et al.*, "A Multi Scale Modeling Approach to Non-Radiative Multi Phonon Transitions at Oxide Defects in MOS Structures," *J.Comp.Elect.*, vol. 11, pp. 218–224, 2012.

[8] C. J. Nicklaw *et al.*, "The Structure, Properties, and Dynamics of Oxygen Vacancies in Amorphous SiO_2," *IEEE Trans.Nucl.Sci.*, vol. 49, pp. 2667–2673, 2002.

[9] G. Kresse *et al.*, "Efficient iterative schemes for ab initio total-energy calculations using a plane-wave basis set," *Phys. Rev. B*, vol. 54, no. 11, pp. 11 169–11 186, 1996.

[10] T. Grasser *et al.*, "On the Microscopic Origin of the Frequency Dependence of Hole Trapping in pMOSFETs," in *Proc. Intl.Electron Devices Meeting*, 2012.

[11] Z.-Y. Lu *et al.*, "Structure, Properties, and Dynamics of Oxygen Vacancies in Amorphous SiO_2," *Phys. Rev. Let.*, vol. 89, p. 285505, Dec 2002.

[12] O. Baumgartner *et al.*, "Modeling of high-k-Metal-Gate-stacks using the non-equilibrium Green's function formalism," in *Proc. Simu.Semicond.Proc.Dev.*, 2008, pp. 353–356.

[13] T. Grasser, "Stochastic charge trapping in oxides: From random telegraph noise to bias temperature instabilities," *Microelectronics Reliability*, vol. 52, no. 1, pp. 39 – 70, 2012.

[14] D. A. Drabold *et al.*, Eds., *Theory of Defects in Semiconductors*. Springer, 2010.

[15] B. R. Tuttle, "Theoretical investigation of the valence-band offset between Si(001) and SiO_2," *Phys. Rev. B*, vol. 70, p. 125322, Sep 2004.

[16] W. Goes *et al.*, "Charging and Discharging of Oxide Defects in Reliability Issues," *Device and Materials Reliability, IEEE Transactions on*, vol. 8, no. 3, pp. 491 –500, sept. 2008.